JACS
JOURNAL OF THE AMERICAN CHEMICAL SOCIETY
pubs.acs.org/JACS
Perspective

# High-Performance Organic Electronic Materials by Contorting Perylene Diimides

Cedric Schaack, Austin M. Evans, Fay Ng, Michael L. Steigerwald, and Colin Nuckolls*

Cite This: J. Am. Chem. Soc. 2022, 144, 42−51
Read Online
ACCESS | Metrics & More | Article Recommendations

**ABSTRACT:** Perylene diimide (PDI) is a workhorse of the organic electronics community. However, the vast majority of designs that include PDI substitute the core with various functional groups to encourage intimate cofacial contacts between largely planar PDIs. Over the past several years, we have observed the counterintuitive result that contorting the planar aromatic core of PDI leads to higher performing photovoltaics, photodetectors, batteries, and other organic electronic devices. In this Perspective, we describe how different modes of contortion can be reliably installed into PDI-based molecules, oligomers, and polymers. We also describe how these different contortions modify the observed optical and electronic properties of PDI. For instance, contorting PDIs into bowls leads to high-efficiency singlet fission materials, while contorting PDIs into helicene-like structures leads to nonlinear amplification of Cotton effects, culminating in the highest *g*-factors so far observed for organic compounds. Finally, we show how these unique optoelectronic properties give rise to higher performance organic electronic devices. We specifically note how the three-dimensional structure of these contorted aromatic molecules is responsible for the enhancements in performance we observe. Throughout this Perspective, we highlight opportunities for continued study in this rapidly developing organic materials frontier.



## INTRODUCTION

This Perspective describes contorted polycyclic aromatic compounds (PACs) based on perylene diimide (PDI) and showcases their use in high-performance organic electronic devices. By virtue of their nonplanarity and $\pi$-conjugation, contorted PDIs have unique optoelectronic characteristics that directly impact their performance in organic electronic devices.[1−8] As we began to prepare contorted, electron-rich aromatics, designing nonplanar PACs was antithetical to the dogma of organic electronics design. Previously, large, flat PACs were regarded as an ideal design for efficient charge transport (Figure 1A). We observed the opposite. We found drastically improved hole mobility in thin-film device performance for contorted PACs compared to their planar analogues.[9,10] Moreover, some contorted aromatics exhibit molecular recognition by virtue of their three-dimensional architecture. For example, a contorted hexabenzocoronene (c-HBC) encapsulates fullerenes, which encourages photoinduced charge separation in photovoltaic devices. We have summarized our findings on these electron-rich c-HBC derivatives before and will therefore not cover them here.[7] In addition, contorted aromatic molecules like cyclophanes, helicenes, or general saddle-shaped PACs have been extensively studied and summarized elsewhere, and we direct the interested reader to the vast and excellent literature on these topics.[11−17] This Perspective does not focus on summarizing molecular contortion as a whole but instead aims to describe the state-of-the-art in contorted perylene diimides, including their materials, properties, and devices, and discuss several directions for future study.

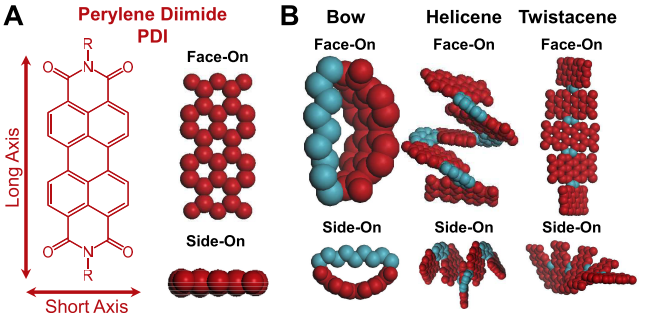


**Figure 1.** (A) Chemical structure and 3D representations of planar PDI. (B) Schematic 3D representations of the bow-, helicene-, and twistacene-shaped contorted PDIs.

Galvanized by our initial successes with the c-HBC series and their design,[18] we began contorting a more versatile PAC, PDI (Figure 1A). PDI is an inexpensive rylene dye[19] and an excellent electron acceptor that is widely used as an industrial pigment. PDIs have been widely studied due to their chemical and photophysical stability, electron-accepting capability, and ease of chemical derivatization.[20] In this Perspective, we describe how contorting PDI in different ways (Figure 1) leads to novel or enhanced material properties over the planar parent compound (Figure 1A). One contortion mode bends PDI

Received: November 1, 2021
Published: December 23, 2021





https://doi.org/10.1021/jacs.1c11544
J. Am. Chem. Soc. 2022, 144, 42−51

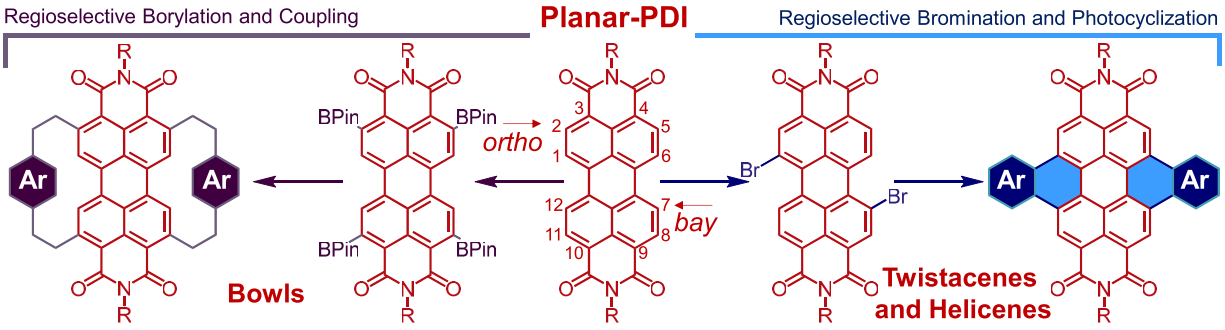


**Figure 2.** Starting from commercial PDI, high-yielding and straightforward transformations afford access to various modes of substitution and resulting contortion. Only the pseudo-*trans* regioisomer of dibrominated PDI is shown for simplicity.

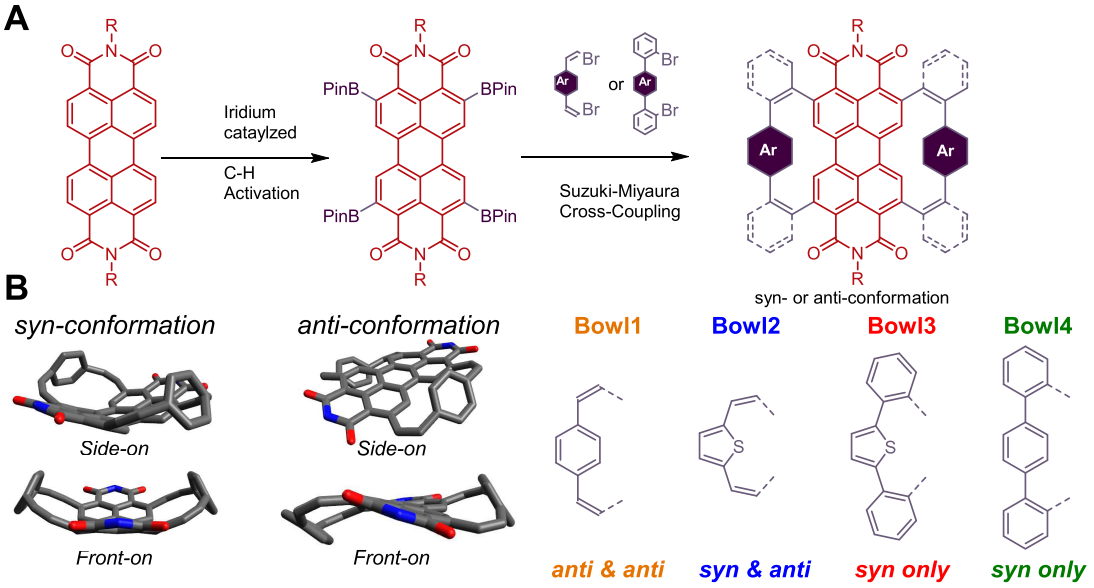


**Figure 3.** (A) Synthesis and structures of **Bowl1**−**Bowl4**. (B) *syn*- and *anti*-conformations of the PDI bowls and a description of which conformers are accessible in each structure. R = $C_{11}H_{23}$ for **Bowl1**−**Bowl2**, $C_5H_{11}$ for **Bowl3**−**Bowl4**.

along its long axis and allows the singlet−triplet energy to be tuned, which leads to increased singlet fission efficiencies. A second mode of contortion twists PDI into deformed ribbons or twistacenes. This nonplanar structure prevents aggregation and encourages intramolecular charge transport, resulting in efficient pseudocapacitors, photodetectors, and state-of-the-art photovoltaic electron acceptors. A third mode introduces contortion along the short axis of PDI, resulting in a well-defined stereogenic axis. To date, this contortion mode has yielded twistacenes and shape-persistent helicene-type structures that have the greatest expression of Cotton effects in electronic circular dichroism (ECD) spectroscopy ever demonstrated for a molecular system (Figure 1B). A fourth mode of PDI contortion, stitching into a strained macrocycle, is also possible, but we have summarized this elsewhere.[21] Collectively, we have shown that contortion enhances the performance of PDI-based organic electronic devices. Below, we detail strategies to contort PDI and describe our recent findings regarding their enhanced optoelectronic properties and organic electronic device performance.

## MOLECULAR DESIGN AND RESULTING PROPERTIES

**Synthetic Approaches toward Contortion of PDI.** A tremendous amount of chemical diversity can be achieved through several high-yielding PDI functionalization strategies. These synthetic methodologies have enabled virtually all of our investigations into contorted PDI materials (Figure 2). First, we find that double bromination of PDI occurs at the bay position (as a mixture of regioisomers);[22,23] second, the photocyclodehydrogenation reaction of acene-linked PDIs regioselectively happens at the bay position;[24,25] and third, borylation using transition metal catalysts occurs at the *ortho*-position, which opens up PDI for various subsequent derivatization methods (Figure 2).[26] The remarkable synthetic versatility of these transformations has generated a wealth of contorted PDI-based aromatics that we discuss in more detail below.

**Contortion of PDI along the Long Axis: Molecular Bowls.** One common method to introduce contortion is by attaching tethers to a planar aromatic molecule (Figure 1B, Figure 2). By careful selection of the parent aromatic core and tether, bent, twisted, and helical contortions can all be reliably embedded into PDI.[2,3,27−33] We recently reported the effect of bending a PDI molecule by tethering two linkers to its ortho positions (2,11 and 5,8 positions) (Figure 3).[34] Preparation of these molecules was achieved by quantitative Ir-catalyzed *ortho*-borylation of PDI and subsequent Pd-catalyzed Suzuki−Miyaura coupling of molecular tethers. Single-crystal X-ray diffraction (SC-XRD) revealed the resulting PDI bowls have


https://doi.org/10.1021/jacs.1c11544
J. Am. Chem. Soc. 2022, 144, 42−51

bending angles of 34° for **Bowl2**, 44° for **Bowl3**, and 45° for **Bowl4** in the solid state (**Bowl1** could not be isolated in its bowl conformation). Through a combination of variable-temperature nuclear magnetic resonance (VT-NMR) spectroscopy and density functional theory (DFT) calculations, we find that **Bowl1** and **Bowl2** are conformationally flexible, interconverting between a bowl and twisted conformation, while **Bowl3** and **Bowl4** are locked into their bowl conformation. Specifically, these observations showed that the *syn*-forms (i.e., the bowl-shaped forms) of **Bowl1** and **Bowl2** were only slightly energetically favored by 1.7 and 4.5–8.0 kcal mol$^{-1}$, respectively, over the *anti*-conformations (i.e., the twisted form). In the case of **Bowl3** and **Bowl4**, the energy difference between *syn*- and *anti*-conformations was >10 kcal mol$^{-1}$, effectively locking the molecules into their bow-shaped isomers. This study highlights a critical, but sometimes overlooked, dynamic structural aspect of contorted aromatic molecules.

Modification of the molecular tethers directly impacts the frontier orbitals and resulting HOMO–LUMO gaps of these contorted PDI-based molecules (Table 1).[34] By increasing the bending angle induced by the tether, we observe an enhanced bathochromic shift in the electronic absorption spectra relative to that of planar PDI (e.g., 50 nm red-shift of the $\lambda_{max}$ between **Bowl1** and **Bowl4**, Figure 4A). Notably, **Bowl1**, **Bowl2**, and **Bowl4** showed similar photoluminescence emission spectra centered at 625, 612, and 617 nm, respectively, while **Bowl3** showed a substantially red-shifted emission centered at 668 nm. Moreover, while **Bowl1**, **Bowl2**, and **Bowl3** exhibited modest fluorescence quantum yields ($\Phi_f$ < 0.01), **Bowl4** showed a substantially enhanced $\Phi_f$ = 0.31, which could be partially due to the reduced conformational flexibility and resultant nonradiative decay modes of **Bowl4**. These changes in the photophysical properties of contorted PDIs were accompanied by modest changes in the reduction potential as evaluated by cyclic voltammetry (Table 1). These experiments demonstrate that the electronic structure of PDI can be systematically modified through molecular contortion.

Bending the PDI along the long axis allows for careful tuning of the excited singlet/triplet energy states, opening a path for the methodical design of singlet fission materials.[35,36] By analyzing molecular orbital maps calculated by DFT calculations, we find that lowering the LUMO energy is a direct consequence of flexing the PDI core (Figure 4B). Specifically, the PDI HOMO (Figure 4B) is found to be a linear combination of two naphthalene imide HOMOs with opposing sign (Figure 4C), which leads to a node where the two halves of this molecule are connected. On the other hand, the LUMO exhibits $\pi$-bonding (i.e., no node) over the two C–C single bonds that connect the two naphthalene imide halves of the PDI core. As such, bending and twisting the PDI has a drastic influence on the LUMO but a much lower impact on the HOMO. By straining the PDI backbone, we find that the singlet fission energies can be tuned (from endoergic, to exoergic, to iso-energetic), leading to over 2 orders of magnitude enhancement in singlet fission rate. These observations naturally signal the need for future investigations focused on stabilizing particular contortion modes in a large library of contorted aromatics, which would provide the first comprehensive comparison among different molecular geometries and emergent photophysical behavior.

**Table 1. Summary of the Optical Properties, Cyclic Voltammetry (CV) Potentials, and Calculated Strain Energies for the Bowl*x* Series, Recorded in $CH_2Cl_2$ ($1 \times 10^{-5}$ M)**

| | absorption | emission | | | |
|---|---|---|---|---|---|
| compound | $\varepsilon$/nm | $\lambda_{em,max}$/nm | $\Phi_f$ | cyclic voltammetry[a]/V | strain energy[b]/kcal mol$^{-1}$ |
| PDI | 525 | 535 | 0.97 | – | – |
| **Bowl1** | 580 | 625 | 0.006 | −3.63 | 30 |
| **Bowl2** | 595 | 612 | 0.009 | −3.70 | 32 |
| **Bowl3** | 595 | 668 | 0.008 | −3.71 | 33 |
| **Bowl4** | 605 | 617 | 0.31 | −3.76 | 42 |

[a]With $Bu_4NPF_6$ (0.1 M) as supporting electrolyte, Ag/AgCl as reference electrode, and the $Fc/Fc^+$ redox couple as an internal standard. [b]DFT calculated values at the B3LYP/6-31G** level of theory.

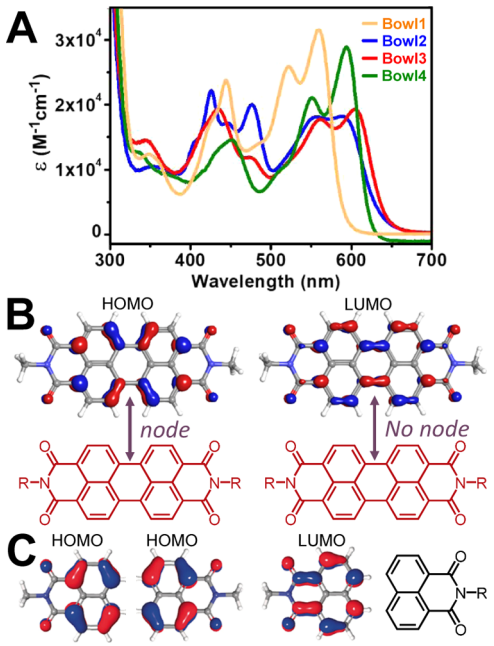


**Figure 4.** (A) UV–vis absorption of PDI bowls in $CH_2Cl_2$ ($1 \times 10^{-5}$ M). (B) Frontier orbitals of PDI and (C) naphthalene imide, effectively half of a PDI. Adapted with permission from ref 34. Copyright 2020 Wiley-VCH Verlag GmbH & Co. KGaA, Weinheim. R = $CH_3$.

**Contortion of PDI along the Short Axis: Helicenes.** Another method to induce contortion into PDI-based molecules is by twisting an aromatic backbone around a stereogenic axis, resulting in helicene-like molecules (Figure 1B). As a class of polycyclic aromatic hydrocarbons, helicenes are notable for their strong UV–vis molar extinction coefficients, while their inherent helical chirality results in strong circular dichroism (CD) responses.[13,37,38] Recent interest has focused on harnessing this circular dissymmetry (the preferential absorption of right- or left-handed circularly polarized light, described as $g = \Delta\varepsilon_{L-R}/\varepsilon$) for organic spin filters, chiral light emitters, and chiral photodetectors, all of which will be critically important for emerging applications in spintronics and quantum information science.[39−41] Typically, the anisotropy and *g*-factors of organic molecules are modest ($10^{-4}$–$10^{-3}$ for typical organic molecules), which is often attributed to size mismatch of molecules (<10 nm) compared


https://doi.org/10.1021/jacs.1c11544
J. Am. Chem. Soc. 2022, 144, 42–51

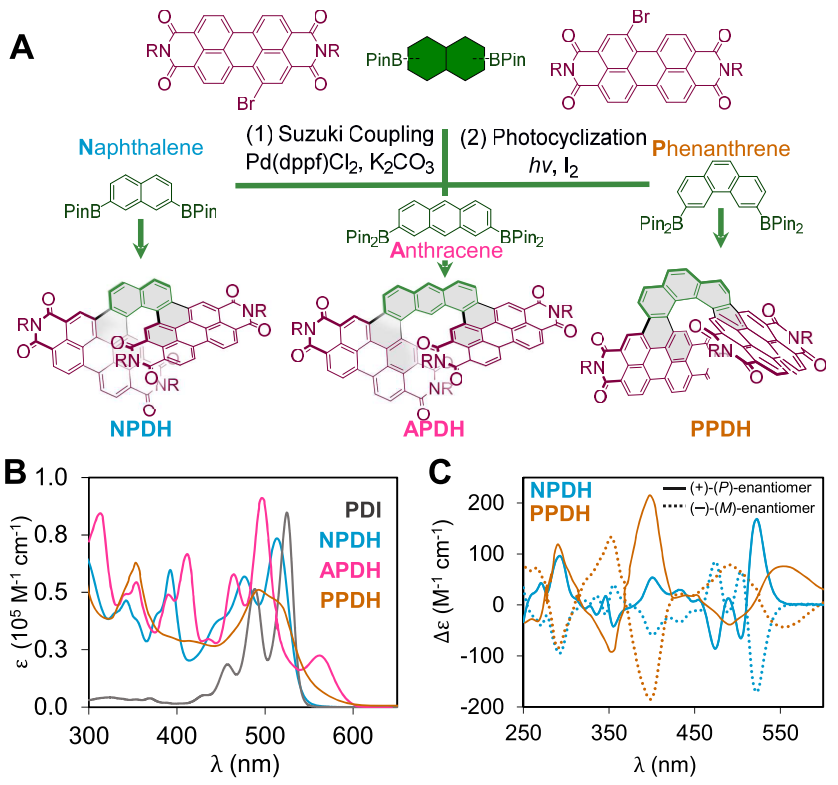


**Figure 5.** (A) Chemical structure of two PDIs helically fused through naphthyl (**NPDH**), anthracenyl (**APDH**), and phenanthrenyl (**PPDH**) acenes. (B) UV−vis and (C) ECD spectra of PDI-based helicenes in $CH_2Cl_2$ ($1 \times 10^{-5}$ M). **APDH** does not show ECD activity due to the lack of stereorigidity. Data are adapted from refs 44 and 45. R = $C_{11}H_{23}$.

**Table 2. Summary of the Optical Properties for the NPDH−NP5H Series, Recorded in $CH_2Cl_2$ ($1 \times 10^{-5}$ M)**

| | $\Delta\varepsilon$/L mol$^{-1}$ cm$^{-1}$ | $\varepsilon$/L mol$^{-1}$ cm$^{-1}$ | | | emission | |
|---|---|---|---|---|---|---|
| compound | 400−425 nm | 350−400 nm | ~500 nm[a] | $\lvert\Delta\varepsilon\rvert/\varepsilon$ maximum | $\lambda_{max,em}$/nm | $\Phi_f$ |
| (*P*)-**PPDH** | 215 | 60 000 | 90 200 | 0.007 | 565 | 0.41 |
| (*P*)-**APDH** | – | 65 000 | 51 000 | – | 575 | – |
| (*P*)-**NPDH** | 168 | 56 900 | 73 100 | 0.002 | 541 | 0.27 |
| (*P*)-**NP3H** | 821 | 95 400 | 102 000 | 0.009 | 549 | 0.44 |
| (*P*)-**NP4H** | 1066 | 104 000 | 103 000 | 0.012 | 551 | 0.58 |
| (*P*)-**NP5H** | 1922 | 160 000 | 127 000 | 0.022 | 553 | 0.68 |

[a]A band at 550 nm is observed for **PPDH** and the larger **NP*x*H** ($x$ = 3−5) with increasing relative intensity compared to the 500 nm band.

to the wavelength of the absorbed light (200−900 nm).[42,43] By engineering helically contorted PDIs, we found that we can surpass the molecular lengths established in other chiral species, and while these molecules remain small compared to the wavelengths of light, we were able to achieve remarkable *g*-factors, as shown below.

We incorporated PDIs into helical scaffolds by fusing two PDI subunits with various acenes, such as naphthyl (**NPDH**), anthracenyl (**APDH**), and phenanthrenyl (**PPDH**) groups (Figure 5A).[23,44,45] The resulting helicenes are highly contorted structures where the length of the fused central acene has a strong influence on the proximity of the two PDI $\pi$-surfaces, impacting the through-space interactions of their respective $\pi$-electron clouds. Markedly, this facilitates intramolecular through-space delocalization between PDI subunits, resulting in significant shifts and molar extinction coefficients of the PDI-centered transitions (Figure 5B).[44,45] **APDH** interconverts between its two helical conformations at room temperature, while **NPDH** and **PPDH** do not interconvert up to >250 °C. Thus, no ECD signal could be observed for **APDH**, while **NPDH** and **PPDH** show strong CD responses (Figure 5C) and encouraging *g*-factors ($|\Delta\varepsilon|/\varepsilon > 10^{-3}$, Table 2). Synthetically, both **NPDH** and **PPDH** show a selectivity for the sterically encumbered products (in agreement with Hückel molecular orbital theory predictions[46]) relative to all other regioisomeric products formed during oxidative photocyclization (Figure 5A). We were interested in further investigating long-range through-space $\pi-\pi$ interactions by expanding dimers into longer oligomers. We elected to focus our study of these oligomeric helicenes on those forged through the naphthyl-based bridge due to the more facile synthetic accessibility of this moiety.[47,48]

Interested to understand the effect of helical PDI length on chiroptical properties, we prepared larger oligomers of **NPDH**. We predicted that molecules of larger size should have stronger interactions with light by reducing the wavelength−molecule size mismatch.[41] We thus prepared a helix-of-helicenes nanoribbon incorporating three PDI units (**NP3H**), which also includes two [6]helicene moieties in its design (Figure 6A).[48] While this did not substantially affect the optical


https://doi.org/10.1021/jacs.1c11544
J. Am. Chem. Soc. 2022, 144, 42−51

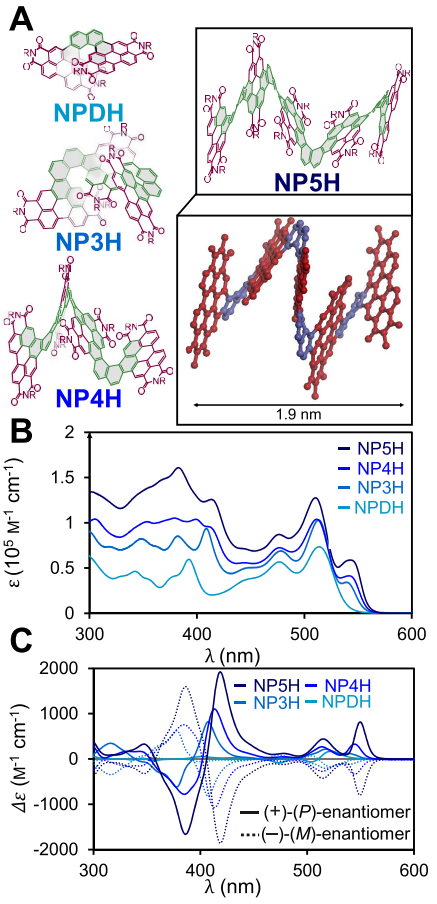


**Figure 6.** (A) Chemical representations of **NP*x*H** ($x$ = 2−5) and a 3D structure derived from the SC-XRD of **NP5H** (protons are omitted for clarity). (B) UV−vis spectra and (C) ECD plots of the **NP*x*H** series in $CH_2Cl_2$ ($1 \times 10^{-5}$ M). Data are from ref 47. R = $C_{11}H_{23}$.

absorption of longer oligomers, the trimer showed more-than-linearly amplified Cotton effects in the ECD spectrum compared to its dimeric analogue **NPDH**, while resulting in dissymmetry $g$-factors of up to $\sim 10^{-2}$ (Table 2 and Figure 6B,C). Our investigations have established the importance of the rigid double [6]helicene moiety on increasing molar extinction coefficients. The largely flat surface of the external PDI moieties leads to the formation of a stacked assembly in SC-XRD (Figure 6A), highlighting the very compact nature of each helicene. Specifically, we found that the helical pitch was substantially reduced from [6]helicene (pitch angle = 58.5°), with internal dihedral angles ranging from 40° to 45°. We have since synthesized extended helicenes up to **NP5H**, incorporating five PDI units linked by four [6]helicenes, the largest such superhelical structure reported so far, with a length of >1.9 nm.[47] This molecule exhibits an interesting structural feature, where naturally occurring clefts originate from the helical setup, which are filled by the imides of PDI. This work has resulted in even further nonlinear amplification of the trimeric precursor's chiroptical spectral intensities, with molar ECD extinction coefficients $|\Delta\varepsilon| > 1900$ $M^{-1}$ $cm^{-1}$ (Figure 6C) and resulting dissymmetry $g$-factor of 2.2%, a record among chiral organic materials (Table 2).

Theoretical calculations revealed that the nonlinear amplification of the chiroptical properties between **NPDH** and **NP$_3$H** is due to exciton-type coupling between the helicene and PDI moieties.[49] DFT calculations were able to accurately reproduce the amplification of the UV and ECD bands, attributing the ∼400 nm band increase to the PDI subunit and the 500 nm band to the helicene units (Figure 7).

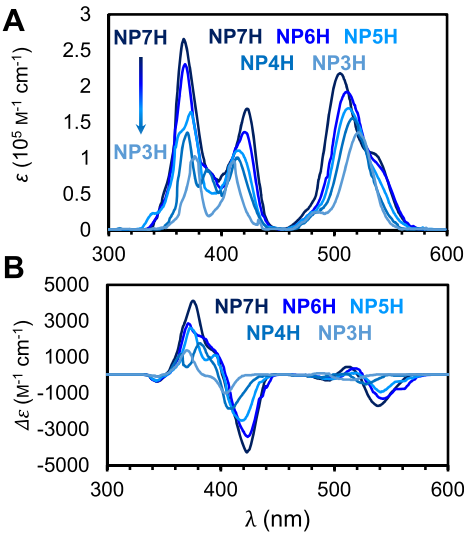


**Figure 7.** (A) Predicted electronic absorption and (B) CD spectra of ($M$)-**NP*x*H** ($x$ = 3, 4, 5, 6, 7). Only (+)-($P$)-enantiomers are shown for clarity. Adapted with permission from ref 49. Copyright 2021 American Chemical Society.

Thus far, our experimental studies have not displayed saturation of chiroptical enhancement (Figure 6B,C). Consistent with this observation, theoretical calculations predict further nonlinear amplification with continued helicene growth. These observations and predictions suggest that the extension of helical PDI-based polymers could lead to unrivaled chiroptical properties that may meet the performance threshold for real-world devices based on these materials.

**Contortion of PDI along the Long Axis: Nanoribbons and Twistacenes.** The final mode of contortion discussed in this Perspective is the bending of PDI strands polymerized along their short axis (Figure 1B). These twisted PDI-based graphene nanoribbons, or twistacenes, can be readily prepared by iterative bromination, aryl coupling, and subsequent oxidative cyclodehydrogenation. Using this chemistry, we developed an efficient synthesis of **hPDI$_2$**, a molecule containing two PDI units fused via an olefin bridge (Figure 8).[50] Early on, we showed that this nonplanar PDI dimer is an excellent electron acceptor and forms $n$-type electron-transporting materials with high thermal stability and high electron mobility. We also showed the simple expansion of our synthetic strategy to three-fused (**hPDI$_3$**) and four-fused PDI units (**hPDI$_4$**) (Figure 8A). Using similar synthetic approaches, we have also prepared push−pull-type ribbons incorporating **hPDI$_2$** and **hPDI$_3$** as electron-accepting moieties linked by an electron-donating pyrene moiety (Figure 8D).[51]

We found that longer oligomers in the **hPDI$_x$** series produce a bathochromic shift in UV absorbance (Figure 8B) and fluorescence emission wavelengths (Figure 8C) while simultaneously showing substantial amplification of molar extinction coefficients and emission intensity (Table 3). In contrast, the push−pull ribbons (Figure 8D) displayed only slight bathochromic shifts compared to **hPDI$_4$** (Table 3). Integrating **hPDI$_2$** in bulk heterojunction (BHJ) solar cells led to an


https://doi.org/10.1021/jacs.1c11544
J. Am. Chem. Soc. 2022, 144, 42−51

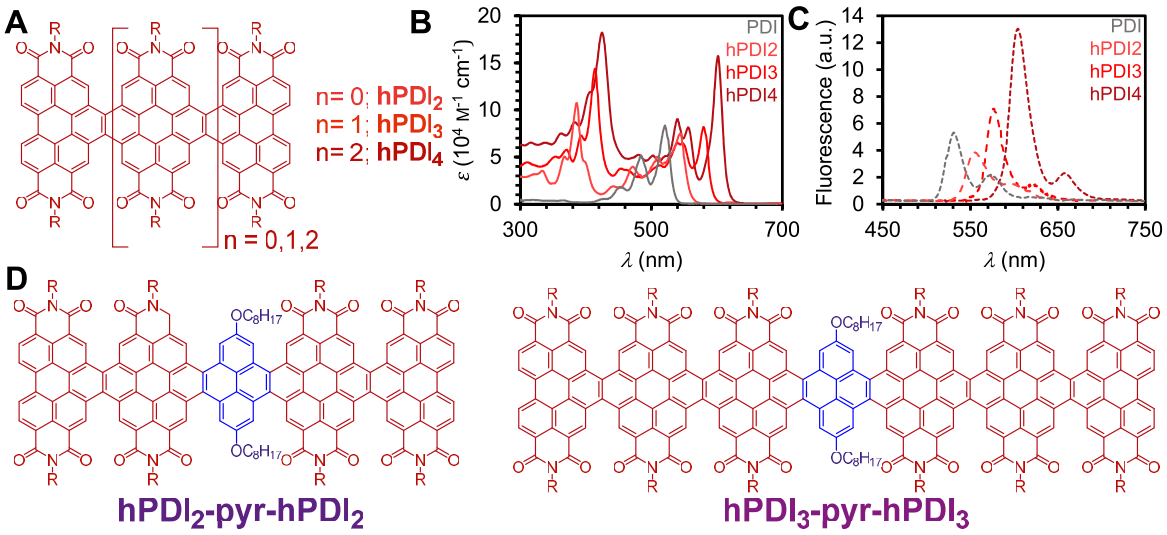


**Figure 8.** (A) Chemical representation of **hPDI$_2$**, **hPDI$_3$**, and **hPDI$_4$** and their (B) electronic absorption and (C) emission spectra in $CH_2Cl_2$ ($1 \times 10^{-5}$ M). Chemical structures of push−pull ribbons, **hPDI$_2$-pyr-hPDI$_2$** and **hPDI$_3$-pyr-hPDI$_3$**. Adapted with permission from ref 50. Copyright 2014 American Chemical Society. R = $C_{11}H_{23}$

**Table 3. Optical and OPV Properties of Contorted PDI and Push−Pull Ribbons**

| | optical properties | | | | | | |
|---|---|---|---|---|---|---|---|
| compound | $\lambda_{max,abs}$/nm | $E_{gap}$/eV | $\lambda_{max,em}$/nm | $\Phi_f$ | PCE/% | FF/% | $J_{SC}$/mA cm$^{-2}$ |
| PDI | 525 | 2.36 | 535 | 0.97 | 0.13[a] | – | – |
| **hPDI$_2$** | 547 | 2.27 | 555 | – | 6.1[a] | 55 | 13.5 |
| **hPDI$_3$** | 580 | 2.14 | 580 | – | 7.9[a] | 67 | 14.3 |
| **hPDI$_4$** | 602 | 2.06 | 610 | – | 8.3[a] | 68 | 15.2 |
| **hPDI$_2$-pyr-hPDI$_2$** | 604 | 2.05 | 660 | 0.5 | 6.9,[b] 14.9[c] | 58.1 | 14.3 |
| **hPDI$_3$-pyr-hPDI$_3$** | 619 | 2.00 | 660 | 0.5 | 7.6,[b] 15.9[c] | 62.9 | 15.1 |

[a]Measured using PTB7-Th as a donor. [b]Measured in a BHJ cell. In a BHJ design, the electron transport material (PDI) and hole transport material (PEDOT:PSS) are blended to be in direct contact and then sandwiched between two electrodes. [c]The iPSC configuration uses a three layer p-i-n design, with PDI as an electron transporting material (p), a perovskite hole insulating layer (i), and PEDOT:PSS as a hole transport material (n).

outstanding photon conversion efficiency (PCE) of 6.1%.[52] Longer **hPDI$_x$** oligomers exhibited even higher efficiencies, with a PCE of 8.3% (fill factor FF = 68%) for **hPDI$_4$** (Table 3), which significantly surpasses the leading fullerene-based electron-acceptor, $PC_{61}BM$, which has a PCE of 5.97%.[23,50,53,54] By integrating push−pull pyrene-containing ribbons into an inverted perovskite halide solar cell (iPSC) geometry, we reached PCEs of 14.9% and 15.9% for **hPDI$_2$-pyr-hPDI$_2$** and **hPDI$_3$-pyr-hPDI$_3$**, respectively, which is considerably higher than the 14.2% PCE observed for $PC_{61}BM$. The increase in PCE can be attributed to one major factor: **hPDI$_x$** display substantially larger UV−vis absorption cross-sections than $PC_{61}BM$. In addition, **hPDI$_x$** molecules display dynamic conformational changes, hindering aggregation, and show large electron mobility in thin films (0.04−0.05 cm$^2$ V$^{-1}$ s$^{-1}$ in thin-film transistors). The immense extinction coefficients, tunable absorption wavelengths, and sharp absorption edges we observed for PDI-based ribbons also led us to test these materials as narrow-band photodetectors.[55] We found that spin-cast thin-film photodetectors of **hPDI$_3$-pyrene-hPDI$_3$** have sharp spectral resolution photodetection, with a full width at half-maximum of <20 nm (Figure 9).

This photodetector spectral resolution is equivalent to that of single-crystal perovskites, which is remarkable since these **hPDI$_x$** layers are produced through scalable solution-processing techniques. In addition to their higher performance and ready processability, contorted PDIs have several advantages over substituted fullerenes. First, the cost of PDI, and its functionalized derivatives, is significantly lower than

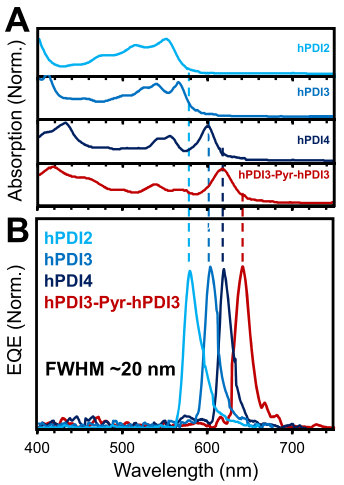


**Figure 9.** (A) Normalized optical absorption spectra of the films in the active layer of the OPD. (B) Normalized external quantum efficiency (EQE) spectra of narrow-band photodetectors made from the PDI-based nanoribbons. Adapted with permission from ref 55. Copyright 2017 American Chemical Society.


https://doi.org/10.1021/jacs.1c11544
J. Am. Chem. Soc. 2022, 144, 42−51

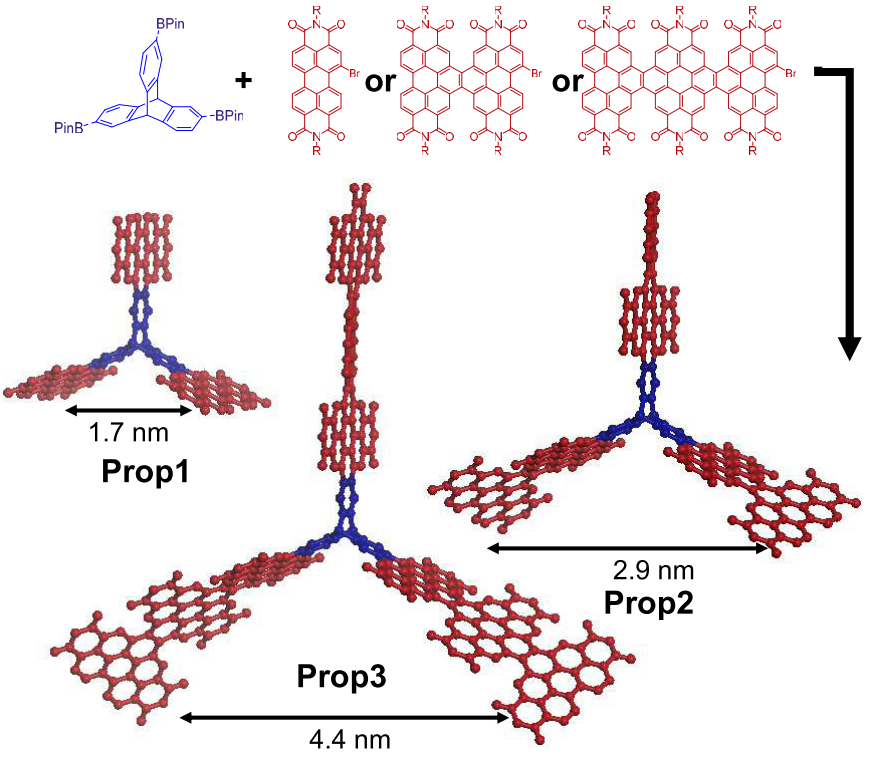


**Figure 10.** Synthetic strategy to access 3D PDI-based nanostructures and the three nanostructures synthesized in this study. R = $C_{11}H_{23}$.

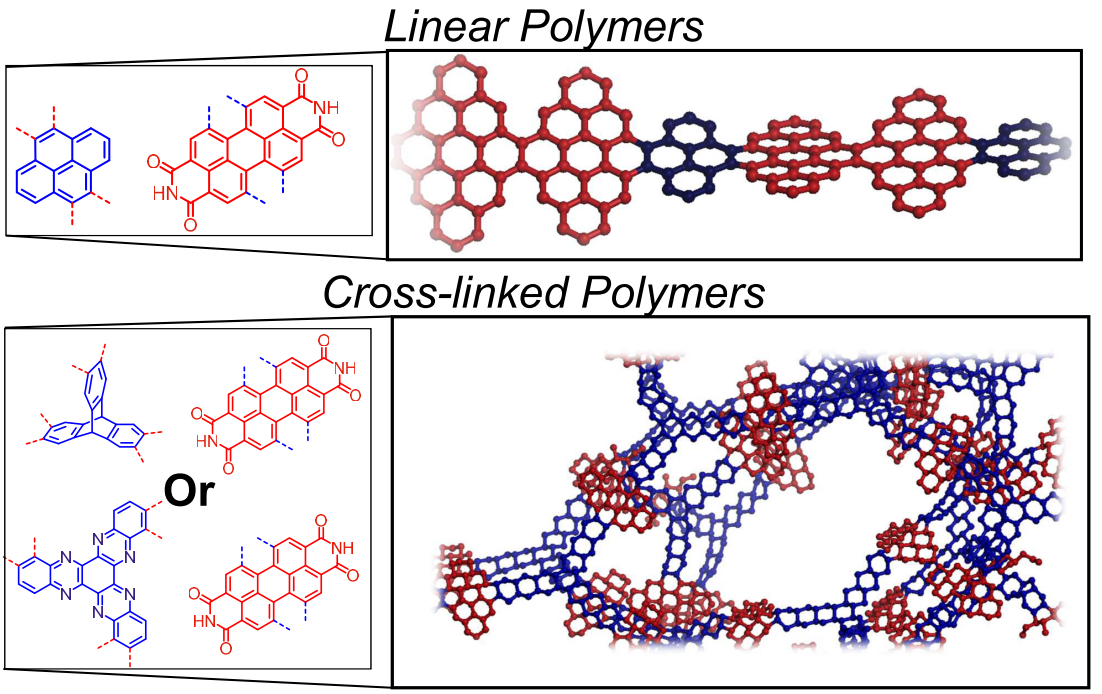


**Figure 11.** Schematic of linear and cross-linked contorted PDI-based polymers.

that of substituted fullerenes. In addition, PDIs are synthetically versatile and can be systematically tuned for particular optical absorbance and emission wavelengths. However, we realized that our earlier investigations into contorted PDIs suggested that conformational flexibility may confound some of these advantages. Driven by these realizations, we were inspired to investigate more rigidly contorted PDIs.

While the **hPDI$_x$** series have three-dimensional waggling structures due to their inherent flexibility, this introduces some heterogeneity in samples of these materials. This inspired us to explore triptycene-based three-dimensional PDIs that are more rigid than the PDI-based twistacenes described above. The resulting propeller-shaped molecules (**Prop1**, **Prop2**, and **Prop3** in analogy to the **hPDI$_x$** fragment incorporated) contained a central triptycene core and three **hPDI$_2$** or **hPDI$_3$** blades fused to it (Figure 10). Fusing three PDIs onto this three-dimensional core led to a 3-fold increase in the molar extinction coefficient compared to that of the analogous


https://doi.org/10.1021/jacs.1c11544
J. Am. Chem. Soc. 2022, 144, 42−51

**hPDI$_3$**. Motivated by the optical behavior and the facile reduction of these species, we explored **Prop*x*** materials as electron-accepting layers in perovskite solar cells. We found that **Prop3** has a record high PCE of 17% in this device architecture, with the smaller **Prop2** displaying a similarly impressive PCE of 16%, well above the efficiencies observed for PC$_{61}$BM. We hypothesize that this increase in PCE is due to the 3D architecture of the propeller-shaped molecule, allowing it to interpenetrate into the perovskite active layer of the solar cell and facilitate charge transport. This finding once again reiterates how careful design of 3D molecular structure can be used to enhance the performance of organic electronic devices.

Having established the utility of contorted PDI small molecules and oligomers, we then became interested in producing polymers of these motifs.[53,56] Our first design focused on the linear polymerization of **pyr-hPDI$_2$** to produce **poly-(pyr-hPDI$_2$)$_n$** (Figure 11). We synthesized the long nanoribbons (up to ∼86 repeat units) by a Suzuki-type polymerization, which is enabled by the inherent solubility of contorted aromatic species. The flexible polymer was subsequently rigidified by regioselective photomediated benzannulation. We then devised a method to post-synthetically remove the solubilizing alkyl chains by quantitative thermolysis, and using this technique, and we prepared devices by solution casting that exhibit high conductivity. This observation inspired us to explore these contorted PDI-based materials as organic pseudocapacitors, which require high electronic and ionic transport. PDI, an exceptionally stable electron acceptor, is well suited to perform as an organic pseudocapacitor active material. To explore this possibility, we synthesized a triptycene-PDI (Figure 11) network polymer, which displayed a large capacitance (350 F g$^{-1}$) at 0.2 A g$^{-1}$ with excellent cycling stability (>10 000 cycles). Consistent with pseudocapacitor behavior, the performance of the pre-annulation material changed from battery-like (high capacitance at low charge rate) to capacitor-like (high charge cycle rate) following annulation. This led to the design of a more planar network polymer based on a **PHATN** (perylene diimide−hexaazatrinaphthylene) motif, which should be able to host even higher charge-storage densities (Figure 11).[55] **PHATN** shows broad, overlapping, and fully reversible CV reduction peaks at −0.7 and −1.0 V versus Hg/HgO. Variable sweep-rate CV measurements revealed the material to resemble a pseudocapacitor, with limited redox shifts up to 50 mV s$^{-1}$, after which the ionic diffusion limit sets in. Pseudocapacitors derived from this material exhibited superlative performance, with tremendous capacitance at low current densities (689 F g$^{-1}$ at 0.5 A g$^{-1}$) and high current densities (430 F g$^{-1}$ at 75 A g$^{-1}$). Overall, we showed that polymeric contorted PDI-based materials are excellent energy storage materials because of their electron-accepting character, inherent stability, and synthetic modularity. Going forward, we expect that significant opportunities exist to improve these designs in terms of cost, cycling stability, energy storage density, solvent compatibility, electrolyte identity, and operating bias.

## CONCLUSION

This Perspective highlights recent advances in contorted aromatic molecules based on perylene diimide and their high-performance organic electronic devices. At the outset of this research program, it seemed counterintuitive to speculate that contorting aromatic motifs could lead to higher organic electronic performance. By intentionally engineering contortion into PDI-based small molecules, oligomers, and polymers, we have produced high-functioning OPVs, OPDs, and organic charge-storage materials. These materials are now surpassing the performance of highly developed inorganic systems such as single-crystal perovskites photodetectors or fullerene-based organic photovoltaics. Throughout these studies, we have shown that contorted organic molecules offer natural advantages in cost, synthetic tunability, and ability to be solution processed. Going forward, fundamental insight into the design rules regarding the cooperative role of contortion and chemical structure on observed optical, electronic, and redox properties must be developed. To aid in this endeavor, the boundaries of molecular contortion should also be expanded. To date, the degrees of contortion and the inherent flexibility are somewhat modest, and we expect that increasing this level of flexibility will lead to even higher performing materials. Central to both of these goals is the development of straightforward chemical functionalization strategies to reliably install desired contortion modes on many molecular motifs. Finally, studies related to thin-film assembly and deposition should be performed, because many solution-processing techniques will likely be well suited to contorted aromatics due to their high solubility. As these challenges are addressed, we expect that organic electronics based on contorted aromatics will find widespread practical usage.

## AUTHOR INFORMATION


### Corresponding Author

**Colin Nuckolls** − *Department of Chemistry, Columbia University, New York, New York 10027, United States;* orcid.org/0000-0002-0384-5493; Email: cn37@columbia.edu

### Authors

**Cedric Schaack** − *Department of Chemistry, Columbia University, New York, New York 10027, United States*

**Austin M. Evans** − *Department of Chemistry, Columbia University, New York, New York 10027, United States;* orcid.org/0000-0002-3597-2454

**Fay Ng** − *Department of Chemistry, Columbia University, New York, New York 10027, United States*

**Michael L. Steigerwald** − *Department of Chemistry, Columbia University, New York, New York 10027, United States*

Complete contact information is available at: https://pubs.acs.org/10.1021/jacs.1c11544


### Notes

The authors declare no competing financial interest.

## ACKNOWLEDGMENTS

Primary support for this research was provided by the National Science Foundation under award DMR-2002634 and the Office of Naval Research under award N00014-16-1-2921. C.S. is supported by NSF CHE-2023568 CCI Phase I: Center for Chemistry with Electric Fields. A.M.E. is supported by the Schmidt Science Fellows, in partnership with the Rhodes Trust. C.N. thanks Sheldon and Dorothea Buckler for their generous support.



https://doi.org/10.1021/jacs.1c11544
J. Am. Chem. Soc. 2022, 144, 42−51

## REFERENCES


(1) Wynberg, H.; Nieuwpoort, W. C.; Jonkman, H. T. Flexible aromatic rings. *Tetrahedron Lett.* **1973**, *14* (46), 4623−4628.
(2) Bodwell, G. J.; Fleming, J. J.; Mannion, M. R.; Miller, D. O. Nonplanar Aromatic Compounds. 3. A Proposed New Strategy for the Synthesis of Buckybowls. Synthesis, Structure and Reactions of [7]-, [8]- and [9](2,7)Pyrenophanes. *J. Org. Chem.* **2000**, *65* (17), 5360−5370.
(3) Bodwell, G. J.; Bridson, J. N.; Cyrañski, M. K.; Kennedy, J. W. J.; Krygowski, T. M.; Mannion, M. R.; Miller, D. O. Nonplanar Aromatic Compounds. 8. Synthesis, Crystal Structures, and Aromaticity Investigations of the 1, n-Dioxa[n](2,7)pyrenophanes. How Does Bending Affect the Cyclic $\pi$-Electron Delocalization of the Pyrene System? *J. Org. Chem.* **2003**, *68* (6), 2089−2098.
(4) Norton, J. E.; Houk, K. N. Electronic Structures and Properties of Twisted Polyacenes. *J. Am. Chem. Soc.* **2005**, *127* (12), 4162−4163.
(5) Sun, C. H.; Lu, G. Q.; Cheng, H. M. Nonplanar Distortions and Strain Energies of Polycyclic Aromatic Hydrocarbons. *J. Phys. Chem. B* **2006**, *110* (10), 4563−4568.
(6) Scott, L. T.; Bronstein, H. E.; Preda, D. V.; Ansems, R. B. M.; Bratcher, M. S.; Hagen, S. Geodesic polyarenes with exposed concave surfaces. *Pure Appl. Chem.* **1999**, *71* (2), 209−219.
(7) Ball, M.; Zhong, Y.; Wu, Y.; Schenck, C.; Ng, F.; Steigerwald, M.; Xiao, S.; Nuckolls, C. Contorted Polycyclic Aromatics. *Acc. Chem. Res.* **2015**, *48* (2), 267−276.
(8) Bedi, A.; Gidron, O. The Consequences of Twisting Nanocarbons: Lessons from Tethered Twisted Acenes. *Acc. Chem. Res.* **2019**, *52* (9), 2482−2490.
(9) Coropceanu, V.; Cornil, J.; da Silva Filho, D. A.; Olivier, Y.; Silbey, R.; Brédas, J.-L. Charge Transport in Organic Semiconductors. *Chem. Rev.* **2007**, *107* (4), 926−952.
(10) Guo, X.; Xiao, S.; Myers, M.; Miao, Q.; Steigerwald, M. L.; Nuckolls, C. Photoresponsive nanoscale columnar transistors. *Proc. Natl. Acad. Sci. U. S. A.* **2009**, *106* (3), 691−696.
(11) Diederich, F. N. From Ansa Compounds to [2.2] Paracyclophane to Cyclophane Complexes. In *Cyclophanes*; The Royal Society of Chemistry, 1991; Chap. 1, pp 1−51.
(12) Rickhaus, M.; Mayor, M.; Juríček, M. Chirality in curved polyaromatic systems. *Chem. Soc. Rev.* **2017**, *46* (6), 1643−1660.
(13) Martin, R. H. The Helicenes. *Angew. Chem., Int. Ed. Engl.* **1974**, *13* (10), 649−660.
(14) Segawa, Y.; Ito, H.; Itami, K. Structurally uniform and atomically precise carbon nanostructures. *Nat. Rev. Mater.* **2016**, *1* (1), 15002.
(15) Scott, L. T. Fragments of fullerenes: Novel syntheses, structures and reactions. *Pure Appl. Chem.* **1996**, *68* (2), 291−300.
(16) Wu, Y.-T.; Siegel, J. S. Aromatic Molecular-Bowl Hydrocarbons: Synthetic Derivatives, Their Structures, and Physical Properties. *Chem. Rev.* **2006**, *106* (12), 4843−4867.
(17) Segawa, Y.; Yagi, A.; Matsui, K.; Itami, K. Design and Synthesis of Carbon Nanotube Segments. *Angew. Chem., Int. Ed.* **2016**, *55* (17), 5136−5158.
(18) Xiao, S.; Myers, M.; Miao, Q.; Sanaur, S.; Pang, K.; Steigerwald, M. L.; Nuckolls, C. Molecular Wires from Contorted Aromatic Compounds. *Angew. Chem., Int. Ed.* **2005**, *44* (45), 7390−7394.
(19) Faulkner, E.; Schwartz, R. J. *High Performance Pigments*, 2nd ed.; Wiley, 2009.
(20) Lee, S. K.; Zu, Y.; Herrmann, A.; Geerts, Y.; Müllen, K.; Bard, A. J. Electrochemistry, Spectroscopy and Electrogenerated Chemiluminescence of Perylene, Terrylene, and Quaterrylene Diimides in Aprotic Solution. *J. Am. Chem. Soc.* **1999**, *121* (14), 3513−3520.
(21) Ball, M.; Zhang, B.; Zhong, Y.; Fowler, B.; Xiao, S.; Ng, F.; Steigerwald, M.; Nuckolls, C. Conjugated Macrocycles in Organic Electronics. *Acc. Chem. Res.* **2019**, *52* (4), 1068−1078.
(22) Rajasingh, P.; Cohen, R.; Shirman, E.; Shimon, L. J. W.; Rybtchinski, B. Selective Bromination of Perylene Diimides under Mild Conditions. *J. Org. Chem.* **2007**, *72* (16), 5973−5979.
(23) Khokhlov, K.; Schuster, N. J.; Ng, F.; Nuckolls, C. Functionalized Helical Building Blocks for Nanoelectronics. *Org. Lett.* **2018**, *20* (7), 1991−1994.
(24) Qiu, W.; Chen, S.; Sun, X.; Liu, Y.; Zhu, D. Suzuki Coupling Reaction of 1,6,7,12-Tetrabromoperylene Bisimide. *Org. Lett.* **2006**, *8* (5), 867−870.
(25) Li, Y.; Xu, L.; Liu, T.; Yu, Y.; Liu, H.; Li, Y.; Zhu, D. Anthraceno-Perylene Bisimides: The Precursor of a New Acene. *Org. Lett.* **2011**, *13* (20), 5692−5695.
(26) Teraoka, T.; Hiroto, S.; Shinokubo, H. Iridium-Catalyzed Direct Tetraborylation of Perylene Bisimides. *Org. Lett.* **2011**, *13* (10), 2532−2535.
(27) Kane, V. V.; Wolf, A. D.; Jones, M. [6]Paracyclophane. *J. Am. Chem. Soc.* **1974**, *96* (8), 2643−2644.
(28) Tobe, Y.; Ueda, K.; Kaneda, T.; Kakiuchi, K.; Odaira, Y.; Kai, Y.; Kasai, N. Synthesis and molecular structure of (Z)-[6]-Paracycloph-3-enes. *J. Am. Chem. Soc.* **1987**, *109* (4), 1136−1144.
(29) Bodwell, G. J.; Bridson, J. N.; Houghton, T. J.; Kennedy, J. W. J.; Mannion, M. R. 1,7-Dioxa[7](2,7)pyrenophane: The Pyrene Moiety Is More Bent than That of C70. *Chem. - Eur. J.* **1999**, *5* (6), 1823−1827.
(30) Bodwell, G. J.; Fleming, J. J.; Miller, D. O. Non-planar aromatic compounds. Part 4: Fine tuning the degree of bend in the pyrene moiety of [7](2,7)pyrenophanes by modifying the nature of the bridge. *Tetrahedron* **2001**, *57* (17), 3577−3585.
(31) Dobrowolski, M. A.; Cyrański, M. K.; Merner, B. L.; Bodwell, G. J.; Wu, J. I.; Schleyer, P. v. R. Interplay of $\pi$-Electron Delocalization and Strain in [n](2,7)Pyrenophanes. *J. Org. Chem.* **2008**, *73* (20), 8001−8009.
(32) Ghasemabadi, P. G.; Yao, T.; Bodwell, G. J. Cyclophanes containing large polycyclic aromatic hydrocarbons. *Chem. Soc. Rev.* **2015**, *44* (18), 6494−6518.
(33) Tsuji, T. Highly Strained Cyclophanes. *Modern Cyclophane Chemistry*; Wiley-VCH Verlag GmbH & Co. KGaA, 2005; pp 81−104.
(34) Liu, T.; Yang, J.; Geyer, F.; Conrad-Burton, F. S.; Hernández Sánchez, R.; Li, H.; Zhu, X.; Nuckolls, C. P.; Steigerwald, M. L.; Xiao, S. Stringing the Perylene Diimide Bow. *Angew. Chem., Int. Ed.* **2020**, *59* (34), 14303−14307.
(35) Conrad-Burton, F. S.; Liu, T.; Geyer, F.; Costantini, R.; Schlaus, A. P.; Spencer, M. S.; Wang, J.; Sánchez, R. H.; Zhang, B.; Xu, Q.; Steigerwald, M. L.; Xiao, S.; Li, H.; Nuckolls, C. P.; Zhu, X. Controlling Singlet Fission by Molecular Contortion. *J. Am. Chem. Soc.* **2019**, *141* (33), 13143−13147.
(36) Smith, M. B.; Michl, J. Singlet Fission. *Chem. Rev.* **2010**, *110* (11), 6891−6936.
(37) Shen, Y.; Chen, C.-F. Helicenes: Synthesis and Applications. *Chem. Rev.* **2012**, *112* (3), 1463−1535.
(38) Gingras, M. One hundred years of helicene chemistry. Part 3: applications and properties of carbohelicenes. *Chem. Soc. Rev.* **2013**, *42* (3), 1051−1095.
(39) Kiran, V.; Mathew, S. P.; Cohen, S. R.; Hernández Delgado, I.; Lacour, J.; Naaman, R. Helicenes—A New Class of Organic Spin Filter. *Adv. Mater.* **2016**, *28* (10), 1957−1962.
(40) Zhang, L.; Song, I.; Ahn, J.; Han, M.; Linares, M.; Surin, M.; Zhang, H.-J.; Oh, J. H.; Lin, J. $\pi$-Extended perylene diimide double-heterohelicenes as ambipolar organic semiconductors for broadband circularly polarized light detection. *Nat. Commun.* **2021**, *12* (1), 142.
(41) Greenfield, J. L.; Wade, J.; Brandt, J. R.; Shi, X.; Penfold, T. J.; Fuchter, M. J. Pathways to increase the dissymmetry in the interaction of chiral light and chiral molecules. *Chem. Sci.* **2021**, *12* (25), 8589−8602.
(42) List, N. H.; Kauczor, J.; Saue, T.; Jensen, H. J. A.; Norman, P. Beyond the electric-dipole approximation: A formulation and implementation of molecular response theory for the description of absorption of electromagnetic field radiation. *J. Chem. Phys.* **2015**, *142* (24), 244111.
(43) Tanaka, H.; Inoue, Y.; Mori, T. Circularly Polarized Luminescence and Circular Dichroisms in Small Organic Molecules:



https://doi.org/10.1021/jacs.1c11544
J. Am. Chem. Soc. 2022, 144, 42−51

Correlation between Excitation and Emission Dissymmetry Factors. *ChemPhotoChem.* **2018**, *2* (5), 386−402.
(44) Schuster, N. J.; Paley, D. W.; Jockusch, S.; Ng, F.; Steigerwald, M. L.; Nuckolls, C. Electron Delocalization in Perylene Diimide Helicenes. *Angew. Chem., Int. Ed.* **2016**, *55* (43), 13519−13523.
(45) Milton, M.; Schuster, N. J.; Paley, D. W.; Hernández Sánchez, R.; Ng, F.; Steigerwald, M. L.; Nuckolls, C. Defying strain in the synthesis of an electroactive bilayer helicene. *Chem. Sci.* **2019**, *10* (4), 1029−1034.
(46) Laarhoven, W. H.; Cuppen, T. J. H. M.; Nivard, R. J. F. Photodehydrocyclizations in stilbene-like compounds. *Recl. Trav. Chim. Pays-Bas* **1968**, *87* (6), 687−698.
(47) Xiao, X.; Pedersen, S. K.; Aranda, D.; Yang, J.; Wiscons, R. A.; Pittelkow, M.; Steigerwald, M. L.; Santoro, F.; Schuster, N. J.; Nuckolls, C. Chirality Amplified: Long, Discrete Helicene Nanoribbons. *J. Am. Chem. Soc.* **2021**, *143* (2), 983−991.
(48) Schuster, N. J.; Hernández Sánchez, R.; Bukharina, D.; Kotov, N. A.; Berova, N.; Ng, F.; Steigerwald, M. L.; Nuckolls, C. A Helicene Nanoribbon with Greatly Amplified Chirality. *J. Am. Chem. Soc.* **2018**, *140* (20), 6235−6239.
(49) Aranda, D.; Schuster, N. J.; Xiao, X.; Ávila Ferrer, F. J.; Santoro, F.; Nuckolls, C. Origin of Chiroptic Amplification in Perylene-Diimide Helicenes. *J. Phys. Chem. C* **2021**, *125* (4), 2554−2564.
(50) Zhong, Y.; Kumar, B.; Oh, S.; Trinh, M. T.; Wu, Y.; Elbert, K.; Li, P.; Zhu, X.; Xiao, S.; Ng, F.; Steigerwald, M. L.; Nuckolls, C. Helical Ribbons for Molecular Electronics. *J. Am. Chem. Soc.* **2014**, *136* (22), 8122−8130.
(51) Sisto, T. J.; Zhong, Y.; Zhang, B.; Trinh, M. T.; Miyata, K.; Zhong, X.; Zhu, X. Y.; Steigerwald, M. L.; Ng, F.; Nuckolls, C. Long, Atomically Precise Donor-Acceptor Cove-Edge Nanoribbons as Electron Acceptors. *J. Am. Chem. Soc.* **2017**, *139* (16), 5648−5651.
(52) Zhong, Y.; Trinh, M. T.; Chen, R.; Purdum, G. E.; Khlyabich, P. P.; Sezen, M.; Oh, S.; Zhu, H.; Fowler, B.; Zhang, B.; Wang, W.; Nam, C.-Y.; Sfeir, M. Y.; Black, C. T.; Steigerwald, M. L.; Loo, Y.-L.; Ng, F.; Zhu, X. Y.; Nuckolls, C. Molecular helices as electron acceptors in high-performance bulk heterojunction solar cells. *Nat. Commun.* **2015**, *6* (1), 8242.
(53) Peurifoy, S. R.; Xu, Q.; May, R.; Gadjieva, N. A.; Sisto, T. J.; Jin, Z.; Marbella, L. E.; Nuckolls, C. Air-stable, long-length, solution-based graphene nanoribbons. *Chem. Sci.* **2020**, *11* (36), 9978−9982.
(54) Chen, W.; Zhang, Q. Recent progress in non-fullerene small molecule acceptors in organic solar cells (OSCs). *J. Mater. Chem. C* **2017**, *5* (6), 1275−1302.
(55) Zhong, Y.; Sisto, T. J.; Zhang, B.; Miyata, K.; Zhu, X. Y.; Steigerwald, M. L.; Ng, F.; Nuckolls, C. Helical Nanoribbons for Ultra-Narrowband Photodetectors. *J. Am. Chem. Soc.* **2017**, *139* (16), 5644−5647.
(56) Russell, J. C.; Posey, V. A.; Gray, J.; May, R.; Reed, D. A.; Zhang, H.; Marbella, L. E.; Steigerwald, M. L.; Yang, Y.; Roy, X.; Nuckolls, C.; Peurifoy, S. R. High-performance organic pseudocapacitors via molecular contortion. *Nat. Mater.* **2021**, *20* (8), 1136−1141.





https://doi.org/10.1021/jacs.1c11544
*J. Am. Chem. Soc.* 2022, 144, 42−51